Equivalent Circuit of a Quadraxial Feed for Ultra-Wide Bandwidth Quadruple-Ridged Flared Horn Antennas

Equivalent Circuit of a Quadraxial Feed for Ultra-Wide Bandwidth Quadruple-Ridged Flared Horn Antennas

Theunis S. Beukman[1], Petrie Meyer[1], Rob Maaskant[2], Marianna V. Ivashina[2]

[1]Department of Electrical and Electronic Engineering, Stellenbosch University, Stellenbosch, South Africa
Email: theunis.beukman@gmail.com; pmeyer@sun.ac.za
[2]Department of Signals and Systems, Chalmers University of Technology, Gothenburg, Sweden
Email: rob.maaskant@chalmers.se; marianna.ivashina@chalmers.se

***Abstract*—An equivalent circuit model of a quadraxial feed for ultra-wide bandwidth quadruple-ridged flared horn (QRFH) antennas is presented. The circuit is synthesised by only 3 unknowns and achieves an accurate input impedance for a wide range of dimensions. This model allows fast synthesis of optimal feeding designs that would ensure the excitation of the fundamental mode at the input of a QRFH.**

***Index Terms*—ultra wideband antennas, quadruple-ridged waveguides, waveguide transitions, equivalent circuits.**

I. Introduction

The transition from one guided wave to another is important for the integration of different microwave devices. Coaxial probes are widely used to couple into rectangular and circular waveguides, with and without ridges [1]. In order to simplify the electromagnetic modelling of these feeding structures, equivalent circuit models are typically derived [2]. In [3] a wideband circuit model is derived for a microstrip-to-slotline transition. This is used to reduce the modelling complexity in the design of a tapered slot antenna array [4].

A quadraxial feeding network was recently proposed for the quadruple-ridged flared horn (QRFH) antenna in [5] by the authors. This feeding technique allows the excitation of the two orthogonal TE_{11} fundamental modes in a circular quad-ridged waveguide (QRWG), required for the wideband dual-polarisation operation of a QRFH antenna [6]. This property is also very attractive to many other antenna and microwave applications [7]. It was shown in [5] that the quadraxial feed improves the antenna performance in terms of cross-polarisation, beamwidth variation and symmetry in the azimuthal planes, as compared to that of a conventional coaxial feed [8].

The differential excitation of the pin pairs in the quadraxial feed is intended for the integration with differential low-noise amplifiers (LNAs). Such a compact solution is attractive for the next-generation radio telescopes which require ultra-low noise performance, hence the necessity for accurate models of the input impedance of the antenna to enable optimal noise matching with the LNAs.

In [5] the focus was on the performance of a quadraxial feed in a QRFH antenna, while in this paper an equivalent circuit model is proposed that gives insight into the operation of such a feed. The model is valid for a single-mode excitation, demonstrated over a band of 2 to 12 GHz, and is also scalable with frequency according to the geometry of the travelling-wave structure.

II. Quadraxial Feed

The QRFH has the useful feature of allowing the separation of the feeding/excitation part from the radiator part. The former consists of the section in which the QRWG is uniform, illustrated in Fig. 1(a), and is referred to as the throat of the horn antenna. The latter is the flaring waveguide part which is consequently referred to as the flared section.

In Fig. 1(b) the back view of the throat is shown where the pins terminate in the ridges. The important dimensions here include the ridge thickness t, the gap between opposing ridges g, the ridge tip width w due to the chamfering that allows a narrow ridge gap, the radius of the pin a_{pin}, the offset distance of the pin from the symmetry axis a_{sep} and the radius of the cylinder in the back wall a_{cyl} where the pins feed through. In Fig. 1(a) a cross-section cut in the yz-plane of the throat is shown. As seen the ridged waveguide is uniform with cylinder radius a_{th} and length L_{th}. The length of the cylinder of the quadraxial line is depicted by L_{cyl}.

There are a few qualitative rules that need to be considered when designing the quadraxial feed:

(i) Each pin should be placed as close as possible to the inner edge of the corresponding ridge to minimise the excitation of higher-order modes.
(ii) The radius of the pin is limited by the ridge thickness – practically each pin has to be inserted into a ridge and therefore cannot exceed this size.
(iii) The radius of the outer conductor of the quadraxial line must be small enough in order to avoid resonances of the TE_{11} mode and to minimise the excitation of higher-order modes in the throat section.

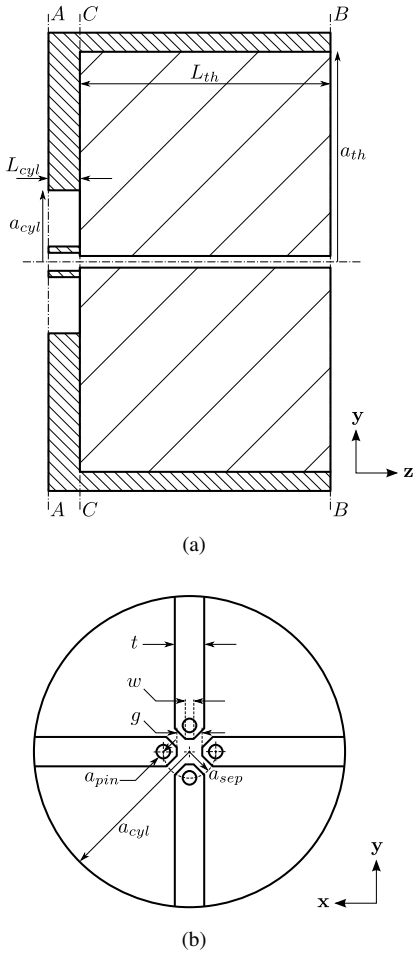

Fig. 1. (a) Cross-section view in the yz-plane of the quadraxial-fed throat. (b) View in the xy-plane of the back of the throat where the pins feed through the wall. Note that the illustration in (b) is scaled up with respect to (a).

For the purposes of this work, the QRFH needs only be excited differentially with two sets of excitations – one exciting the vertically orientated ridges and the other the horizontally orientated ridges. As the two resulting fields are simply rotated versions of each other, two separate and identical circuit models can be constructed. To set up a field solution corresponding to one of these excitations in Computer Simulation Technology's Microwave Studio (CST-MWS), the structure in Fig. 1 is terminated at plane B-B with a waveguide port allowing for all the propagating modes, and at plane A-A with a multi-pin feed exciting only two opposing pins differentially.

In order to evaluate the proposed circuit model, two different QRWGs are employed. The dimensions of these uniform waveguides are based on the throat sections of two existing QRFH antennas which were both designed for dual-reflector systems with similar subtended angles. The first throat, referred to as $Throat1$, is based on the parameter studies reported in [9] for a preliminary QRFH design for Band 1 of SKA-mid, which covers a 3:1 bandwidth from 0.35 to 1.05 GHz. The second throat ($Throat2$) consists

TABLE I. The coaxial-fed impedances and ridged waveguide dimensions (as depicted in Fig. 1) of $Throat1$ and $Throat2$.

Parameter	$Throat1$	$Throat2$
Z_0	$100\ \Omega$	$50\ \Omega$
a_{th}	$33.55\ mm$	$28.05\ mm$
g	$1.87\ mm$	$1.3\ mm$
t	$2.15\ mm$	$3\ mm$
w	$0.61\ mm$	$0.51\ mm$

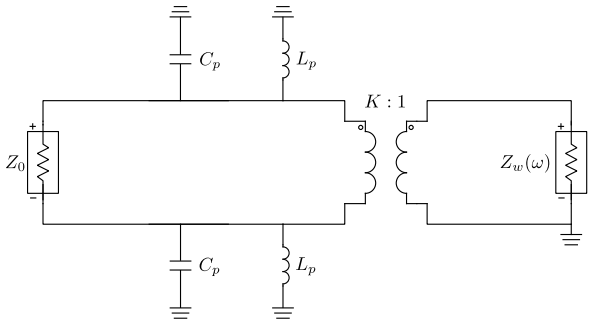

Fig. 2. Equivalent circuit model for the transition from the differential TEM mode in the quadraxial line to the TE_{11} mode in the QRWG.

of the dimensions reported in [8] for a QRFH with a 6:1 bandwidth from 2 to 12 GHz. The parameter values of these QRWGs are given in Table I. Note that the dimensions reported for $Throat1$ are scaled from its lowest frequency $f_{lo} = 0.35\ GHz$ to the band of interest of this work where $f_{lo} = 2\ GHz$.

III. Equivalent Circuit Model

The proposed equivalent circuit for one differential excitation of the quadraxial feed is shown in Fig. 2. As discussed, the exact same circuit also holds for the second differential excitation of the quadraxial feed, which is simply the first excitation rotated by $90°$. The circuit consists of an impedance transformer with winding ratio K:1 which transforms the impedance of the differential TEM mode (Z_0) in the quadraxial line to the impedance of the TE_{11} mode (Z_w) in the QRWG, and shunt elements L_p and C_p which models the reactive fields generated at the discontinuity formed by the transition from the quadraxial line to the QRWG. Note that this model is only valid if the implementation of the quadraxial feed adheres to the design rules listed in Section II.

The transformer ratio is simply calculated as

$$K = \sqrt{\frac{R_{eq}}{\eta_0}}, \tag{1}$$

where

$$R_{eq} = \frac{1}{\mathfrak{Re}\{Y_e\}} \tag{2}$$

and Y_e is the input admittance as seen from the pins, referred to plane C-C, and averaged over the frequency range of single-mode TE_{11} propagation. This admittance typically has a frequency dependent susceptance while the conductance

TABLE II. The quadraxial feed dimensions as depicted in Fig. 1.

Parameter	Value
a_{pin}	$0.5\ mm$
a_{cyl}	$11.4\ mm$
L_{cyl}	$3.5\ mm$
a_{sep}	equation (3)

is near constant over frequency and mostly influenced by the dimensions of the ridged waveguide. The parameter η_0 represents the intrinsic wave impedance of free-space which is 377 Ω. The latter is chosen due to the fact that as the frequency increases above cut-off the wave impedance of a mode tends to 377 Ω. This is found to be more effective than using the actual wave impedance of TE_{11}, which would make the value of K dependent on frequency.

To illustrate the dependencies of the different circuit components on the physical dimensions, the quadraxial feed is implemented in $Throat1$ and $Throat2$. The dimensions are chosen according to Table II and the length of the line is de-embedded in the simulation, in order to consider the transition alone. The pin offset is calculated as

$$a_{sep} = (g/2 + t/4 + a_{pin}) \tag{3}$$

to ensure that design rule (i) in Section II is satisfied. All three the component values in Fig. 2 are empirically extracted from the input impedance of the full-wave simulation.

The values of the equivalent resistance R_{eq} are plotted in Fig. 3(a) for different values of the ridge dimensions g and t. Here it is clearly seen that as the gap narrows between the ridges the equivalent resistance becomes smaller, while a thinner ridge has the opposite affect. Note that the only geometrical differences here between $Throat1$ and $Throat2$ are the cylindrical diameters a_{th} (i.e. respectively 33.55 and 28.05 mm) and the tip widths of the ridges w (i.e. respectively 0.61 and 0.51 mm). Thus, $Throat1$ has a smaller equivalent resistance than $Throat2$ due to its larger distributed capacitance caused by the larger tip width of the ridges, observed in Fig. 3(a). As expected, the equivalent resistances of these two throat sections are almost equal to the respective characteristic impedances of their designed coaxial feeds given in Table I – i.e. $Z_0 \approx R_{eq}$. Furthermore, it is found that only the dimensions of the ridged waveguide have a significant influence on R_{eq}.

The inductance L_p in the circuit model is almost linearly dependant on the diameter of the outer conductor of the quadraxial line a_{cyl}, whereas C_p is essentially constant, as shown in Figs. 3(b) and 4(a). Therefore, the physical interpretation of L_p is that the section of the back of the ridge where the quadraxial line terminates – i.e. between a single pin and the outer conductor [see Fig. 1(b)] – forms a distributed inductance which is dependent on the length $(a_{cyl} - a_{sep})$. The ridge thickness also has some influence on this inductance. The slight differences between the values obtained for the two throats can be ascribed to the fact that the ridge gap is larger in $Throat1$ and therefore effectively reduces the inductance L_p compared to $Throat2$.

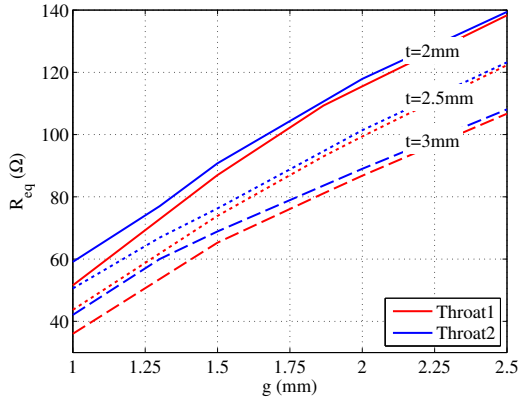

(a)

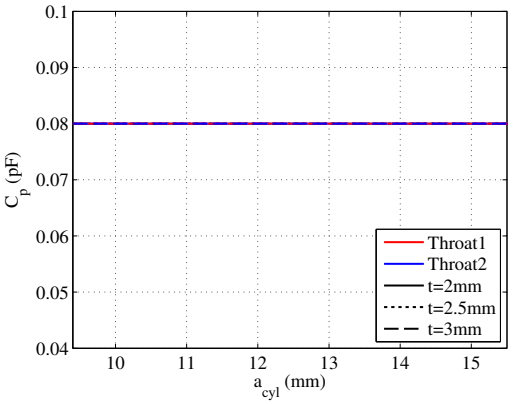

(b)

Fig. 3. The values of the circuit components (a) R_{eq} and (b) C_p for different simulation dimensions.

This simple inductance model is valid for short transition regions only. For longer regions, Fig 4(b) shows the dependence of L_p on the physical length L_{cyl}, for the instance where $a_{cyl} = 11.4\ mm$. The different values for t have similar influences on L_p as in Fig. 4(a). Therefore, it is reasonable to conclude that the inductance component is dependent on the physical path of the current from the point where the pins terminate in the ridges to the grounded part of the multi-pin port.

Finally, a_{pin} and a_{sep} do not have any significant influence on the equivalent circuit as long as the design rules in Section II are applied. The throat length L_{th} can be of arbitrary length due to the ideal modal termination of the waveguide port. In the simulation setup this should however be long enough so that the reactive power of the evanescent modes does not influence the S-parameter results.

IV. Performance

To illustrate the accuracy of the equivalent circuit model, Γ_{in} of a few different quadraxial-fed throat sections are plotted in Fig. 5. The dimensions in Tables I and II are used with variations of a_{cyl} and t. Good agreement is found between

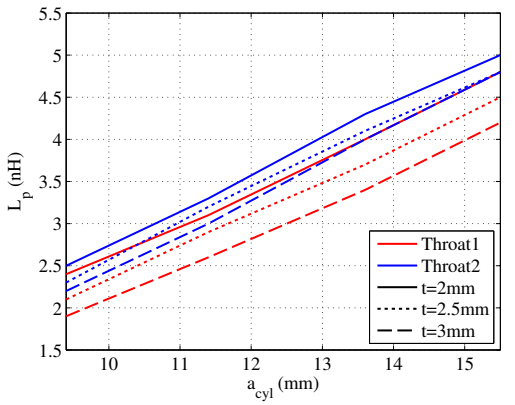

(a)

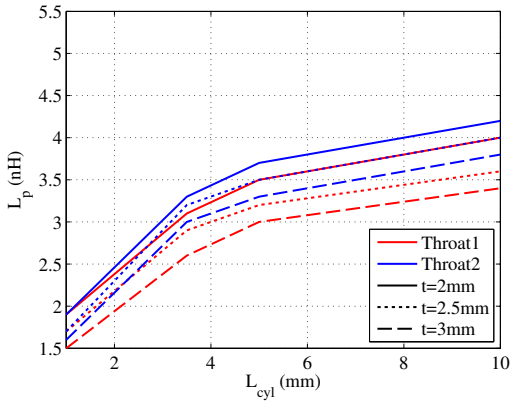

(b)

Fig. 4. The values of the circuit component L_p for different simulation dimensions.

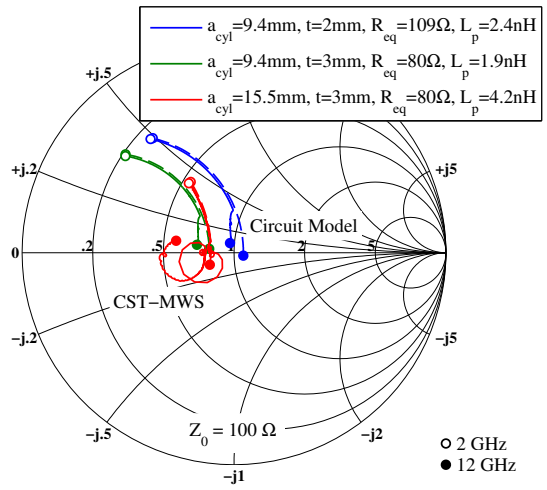

(a)

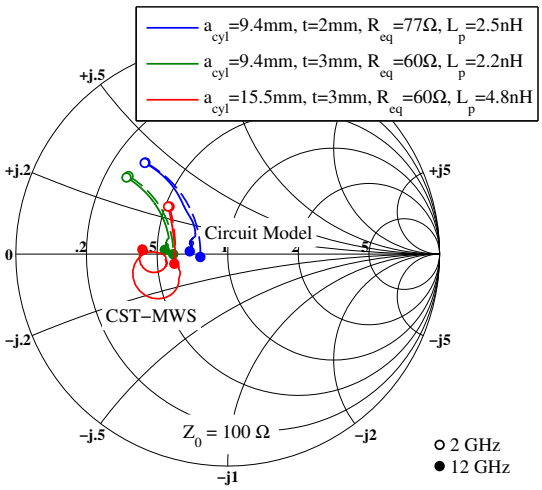

(b)

Fig. 5. The input impedances of (a) $Throat1$ and (b) $Throat2$ for different dimension sets. The CST-MWS simulation is depicted by the solid line and the corresponding circuit model by the dashed line.

the CST-MWS simulation and the circuit model; however, at the highest frequencies there exist some deviations and more significantly so for the instance where $a_{cyl} = 15.5\ mm$. This is due to the excitation of higher-order modes such as TE_{31}, TM_{11}, TE_{32} and TE_{13} – with TM_{11} being the strongest amongst these. Note that TE_{32} and TE_{13} are below cut-off in $Throat2$. Therefore, by implication the importance of design rule (iii) is observed.

To model the effects of higher-order modes, the simple single-mode circuit model evidently becomes insufficient, and models incorporating higher-order modes become necessary. One such model represents each mode as a separate waveguide port, with possibly complex transformer ratios [10]. For the purposes of this work – where single-mode excitation of the throat sections is desired over wide bandwidths – the single-mode circuit model is however more useful for optimisation with less complexity, given that the design rules are satisfied.

A trade-off exists between the modal purity and the input match. In order to avoid the excitation of unwanted higher-order modes, the radius a_{cyl} should be sufficiently small; however, this decreases the distributed inductance L_p of the transition and results in a poorer input match at the lowest frequencies. It is found for both $Throat1$ and $Throat2$ that a radius of $11.4\ mm$ is a good trade-off.

Furthermore, the differential impedance of the quadraxial line is generally high compared to the values of R_{eq} given in Fig. 3(a), due to the constraints of the realisable gap and typical thickness of ridges, on the placement and size of the quadraxial line. Therefore the input matches in Fig. 5 are degraded when the line length L_{cyl} is not de-embedded.

The input match could however be improved by inserting a dielectric material in the quadraxial line, in order to reduce its characteristic impedance. In this case the equivalent circuit is still applicable, although the component values in Figs. 3 and 4 would change.

V. Conclusion

A simple equivalent circuit model is proposed for the transition from a quadraxial line to a quadruple-ridged waveguide. This model gives insight into the operation of the feed and is beneficial for the purpose of achieving an optimal design, without having to run time consuming full-wave simulations. The modal purity in the throat does limit the accuracy of the circuit; however, for the purpose of exciting QRFHs, only the fundamental mode is desired.

Acknowledgement

The authors would like to acknowledge the SKA South Africa and NRF South Africa as well as the Swedish VR and VINNOVA agencies, for funding this work.

References

[1] S. B. Cohn, "Design of simple broad-band wave-guide-to-coaxial-line junctions," *Proceedings of the IRE*, vol. 35, no. 9, pp. 920–926, September 1947.

[2] M. D. Deshpande and B. N. Das, "Analysis of an end launcher for a circular cylindrical waveguide," *IEEE Transactions on Microwave Theory and Techniques*, vol. 26, no. 9, pp. 672–675, September 1978.

[3] M. V. Ivashina, E. A. Redkina, and R. Maaskant, "An accurate model of a wide-band microstrip feed for slot antenna arrays," in *Antennas and Propagation Society International Symposium*, June 2007, pp. 1953–1956.

[4] R. Maaskant, M. V. Ivashina, O. Iupikov, E. A. Redkina, S. Kasturi, and D. H. Schaubert, "Analysis of large microstrip-fed tapered slot antenna arrays by combining electrodynamic and quasi-static field models," *IEEE Transactions on Antennas and Propagation*, vol. 59, no. 6, pp. 1798–1807, June 2011.

[5] T. S. Beukman, M. V. Ivashina, R. Maaskant, P. Meyer, and C. Bencivenni, "A quadraxial feed for ultra-wide bandwidth quadruple-ridged flared horn antennas," in *The 8th European Conference on Antennas and Propagation (EuCAP)*, The Hague, The Netherlands, April 2014.

[6] T. S. Beukman, P. Meyer, M. V. Ivashina, R. Maaskant, and D. I. L. de Villiers, "Modal considerations for synthesizing the tapering profile of a quadruple-ridged flared horn antenna," in *International Conference on Electromagnetics in Advanced Applications (ICEAA)*, Palm Beach, Aruba, August 2014.

[7] W. Sun and C. A. Balanis, "Analysis and design of quadruple-ridged waveguides," *IEEE Transactions on Microwave Theory and Techniques*, vol. 42, no. 12, pp. 2201–2207, December 1994.

[8] A. Akgiray, S. Weinreb, W. Imbriale, and C. Beaudoin, "Circular quadruple-ridged flared horn achieving near-constant beamwidth over multioctave bandwidth: Design and measurements," *IEEE Transactions on Antennas and Propagation*, vol. 61, no. 3, pp. 1099–1108, March 2013.

[9] C. Bencivenni, "0.35-1.05 GHz quadruple-ridge flared horn feed for the square kilometre array radio telescope," Onsala Space Observatory, Sweden, Tech. Rep. Rev. 1, 2013.

[10] C. A. W. Vale and P. Meyer, "Automated intelligent mode selection for fast mode matching analysis of waveguide discontinuities," in *IEEE MTT-S International Microwave Symposium*, Phoenix, USA, May 2001.